InAs/InP quantum dot mode-locked laser with an aggregate 12.544 Tbit/s transmission capacity

Liu, Guocheng; Poole, Philip J.; Lu, Zhenguo; Liu, Jiaren; Mao, Youxin; Vachon, Martin; Barrios, Pedro

Publisher's version / Version de l'éditeur:
https://doi.org/10.1364/OE.441820
Optics Express, 30, 3, pp. 3205-3213, 2022-01-31

Research Article Vol. 30, No. 3 / 31 Jan 2022 / Optics Express 3205
Optics EXPRESS

InAs/InP quantum dot mode-locked laser with an aggregate 12.544 Tbit/s transmission capacity

GUOCHENG LIU,* PHILIP J. POOLE, ZHENGUO LU, JIAREN LIU, YOUXIN MAO, MARTIN VACHON, AND PEDRO BARRIOS

Advanced Electronics and Photonics Research Centre, National Research Council, Ottawa, ON, Canada
guocheng.liu@nrc-cnrc.gc.ca

Abstract: Chip-scale optical frequency comb sources are ideal compact solutions to generate high speed optical pulses for applications in wavelength division multiplexing (WDM) and high-speed optical signal processing. Our previous studies have concentrated on the use of quantum dash based lasers, but here we present results from an InAs/InP quantum dot (QDot) *C*-band passively mode-locked laser (MLL) for frequency comb generation. By using this single-section QDot-MLL we demonstrate an aggregate line rate of 12.544 Tbit/s 16QAM data transmission capacity for both back-to-back (B2B) and over 100-km of standard single mode fiber (SSMF). This finding highlights the viability for InAs/InP QDot lasers to be used as a low-cost optical source for large-scale networks.

1. Introduction

The global optical fiber network carries hundreds of Tbit/s with ~25% annual capacity growth in bandwidth [1]. The use of WDM and advanced modulation formats [2–4] is becoming more and more attractive to alleviate transmission bottlenecks. Particularly, mutually coherent optical carriers can be applied to generate *superchannels* for optical communication applications and high-speed data transmission [5,6]. Besides higher data rate, a compact, low-cost, energy-efficient chip-scale optical frequency comb source is also desired for offering tens or even hundreds of well-defined narrowband optical carriers used to carry digital data. This source would replace the use of many individual lasers. Various chip-scale frequency comb sources have been demonstrated for WDM data transmission at Tbit/s data rates, such as employing soliton comb generation in micro-resonators or dark soliton comb generation [1,2,7,8]. These techniques can provide a large number of comb lines, and hybrid integration [9,10] of these comb sources with other photonic components could provide a potential solution for the WDM sources. However, the techniques are challenged by low power conversion efficiency of these comb sources, which leads to low power per comb line thus low optical signal-to-noise ratio level [10,11]. Electro-optic (EO) combs offer wide-band and agile tuning of the mode spacing [12]. Utilizing a thin-film lithium niobate platform, a broadband EO frequency comb [13] exhibited excellent configurability and stability as a powerful complement to integrate with Kerr combs. However, the EO combs have comparatively high complexity associated with driving a multitude of modulators with RF signals of precisely defined amplitude and phase [14]. Gain-switched laser diodes may be integrated into chip-scale packages with all peripheral components. However, the overall transmission performance can be limited by the line spacing and the available number of lines [5,15].

These limitations may be overcome by quantum-dot (QDot) and dash (QDash) based single-section semiconductor mode-locked lasers (MLLs) [16–18]. These devices are a promising solution for next generation high speed optical networks and optical signal processing [16] due to their advantages such as stable optical pulses at high repetition rates, narrow pulse widths, compact size, low power consumption, simple fabrication, and the potential for hybrid integration with silicon substrates [19–21]. Moreover, they offer reduced spontaneous emission rates and

#441820 https://doi.org/10.1364/OE.441820
Journal © 2022 Received 31 Aug 2021; revised 12 Dec 2021; accepted 14 Dec 2021; published 18 Jan 2022

Optics EXPRESS

low threshold current densities which lead to reduced intrinsic noise [16,22]. These very simple Fabry-Perot lasers support multiple longitudinal lasing modes, with all the modes mutually phase locked [23], allowing extremely high repetition rates. This is all possible without the requirement for saturable absorbers, complex design, and delicate control of multiple electrical contacts [24,25]. These lasers exhibit optical linewidths (measured over a time frame >> μs) in the MHz range which can limit the transmission performance, especially at low symbol rates [26]. On the other hand the linewidth observed over a very short time frame, the radio-frequency (RF) linewidth [27] and the differential phase noise between adjacent comb lines are much smaller, showing high coherence among these spectral lines thus enabling complex modulation formats [28,29] and joint phase estimation [2].

Various demonstrations have been carried out to show the potential of single-section QDot and QDash mode locked lasers for Tbit/s transmission [22,26,27,29–39], such as an aggregate line rate of 11.55 Tbit/s reported on 16QAM dual-polarization 75-km SSMF WDM transmission using 38 channels of a QDash-MLL [26]. By exploiting feedback from an external-cavity, an increased aggregate line rate of 12 Tbit/s on 32QAM WDM transmission could be reached [34]. However, external feedback schemes make the setup more complicated, which may result in undesirable phenomena such as mode instability or hopping, which would be detrimental for the BER performance in data transmission [40].

In recent years we have reported several InAs/InP QDot and QDash-MLLs operating in the *C*- and *L*-band with channel spacings from tens of GHz to THz [17,18,27,37–39,41–43], focusing on the performance of QDash based lasers for high speed data communications. Compared to their QDash counterparts, it has been suggested that QDots are favorable for lasers as the improved height-diameter aspect provides a deeper confinement of the charge carriers [44]. QDot lasers have been shown to exhibit larger values of direct modulation bandwidth and relaxation oscillation frequency induced by the fast carrier capture from the wetting layer to the dots [45–47]. In our group we have also consistently observed shorter pulse durations with mode-locked QDot based lasers as compared to QDash, indicating improved mode-locking. Therefore, in this paper we study in detail the behavior of QDot rather than QDash based InAs/InP MLLs, without the use of external optical feedback. We look at three different cavity length devices. The influences of the cavity lengths on the optical lasing spectra and RF mode beating spectra are investigated. We study in more detail the performance of the laser with a mode spacing of 28.45 GHz. In particular the relative intensity noise (RIN), phase noise, and data transmission characteristics using 16QAM at 28-GBd are studied. Using this laser we demonstrate 12.544 Tbit/s (16QAM 56×28-GBd PDM) aggregate line-rate data transmission capacity for both back-to-back (B2B) and over 100-km of SSMF.

2. Experimental configuration

The InAs/InP QDot material was grown on 3" (001)-oriented *n*-type InP substrates by chemical beam epitaxy (CBE) with metal organic chemical vapour deposition (MOCVD) used to grow the top *p*-type cladding layers. A 355 nm thick InGaAsP waveguide core contained five stacked layers of InAs QDots with lattice matched $In_{0.816}Ga_{0.184}As_{0.392}P_{0.608}$ (1.15Q) barriers as the gain medium, providing both carrier and optical confinement, surrounded by *n*- and *p*- type InP cladding layers. A double cap process was used to precisely control the emission wavelength [41]. The average QDot density was approximately 3.5×10^{10} cm^{-2} per layer. We can choose to grow either QDots or QDashes as the gain medium through adjustments in the growth conditions [48]. For the InAs QDashes used in earlier reports [27,32,37,38] we deposited the InAs with a low As flux on a thin GaAs layer. To grow the InAs QDots [41] for this study we replaced the thin GaAs layer with GaP, doubled the As flux for the InAs deposition, and increased the growth temperature by 10°C. Single lateral mode ridge waveguide QDot-MLLs were fabricated with a ridge width of 2.3 μm via standard photolithography and combination of dry-, wet-etching

Optics EXPRESS

and contact metallization techniques. Cavity lengths of 1000 μm, 1500 μm, and 2000 μm were cleaved and the facets were left uncoated.

Figure 1(a) shows a schematic cross-section of the device, while a corresponding scanning electron microscope (SEM) image of the facet of a processed laser is shown in Fig. 1(c). Figure 1(b) shows a SEM image of a surface dot layer grown under the same conditions used for the laser. The cleaved laser bars were placed directly on a copper block (without any physical bonding), DC-driven with an ultra-low noise laser driver, and temperature was maintained at 17°C by a thermo-electric cooler and controller (ILX Lightwave, Model LDC-3724C). The laser output was collected by an antireflection coated lensed fiber followed by a two-stage optical isolator (isolation >60 dB) to prevent any residual optical feedback into the laser cavity. To study the passive mode-locking behavior of the laser, the output spectrum was characterized using an optical spectrum analyzer (OSA) (Ando, Model AQ6317B), RF performance was measured using a 50 GHz PXA signal analyzer (Keysight Technologies, Model N9030A) with a 45 GHz IR photodetector (New Focus, Model 1014), and RIN and phase noise were measured with an Agilent N4371A relative intensity noise measurement system and an OE4000 automated laser linewidth/phase noise measurement system (OEWaves Inc.).

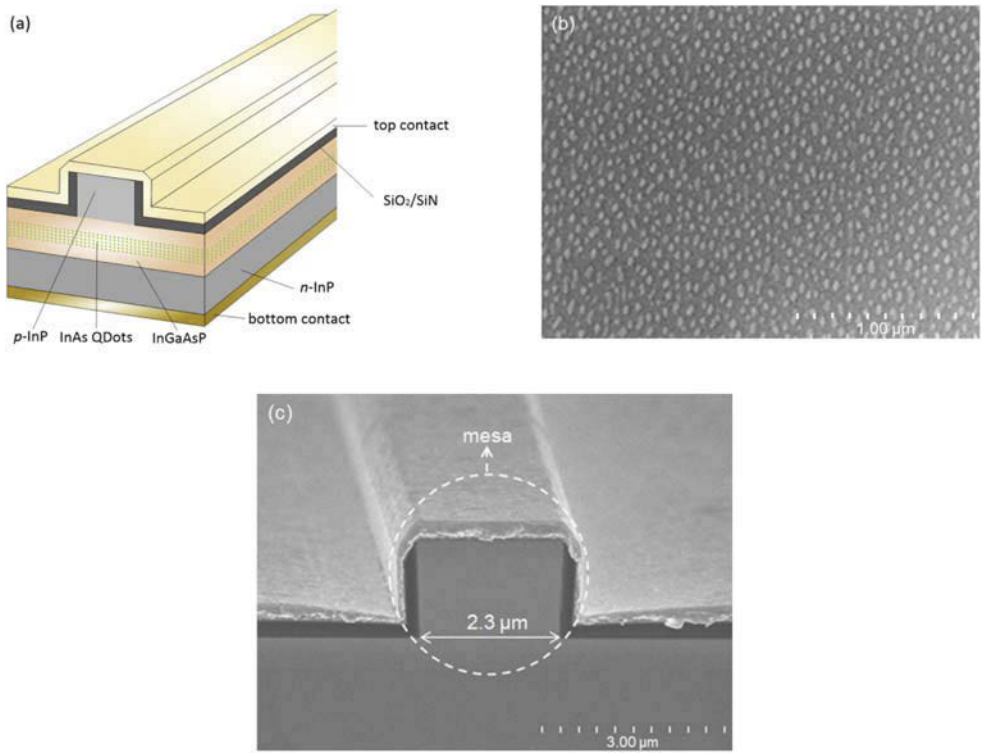

Fig. 1. (a) Schematic cross-sectional diagram of a shallow-etched ridge-waveguide InAs/InP QDot laser; (b) Scanning electron microscopy of the top view of the InAs QDot layer; and (c) Cross-sectional scanning electron microscopy image showing the facet of a fabricated Fabry-Perot InAs/InP QDot laser.

The QDot-MLL with a 1500 μm cavity length emitted a multi-wavelength comb within the *C*-band. Each wavelength channel of the comb was selected by an optical bandpass filter (OBPF) (Santec, Model OTF-350) as an optical carrier and an erbium-doped optical fiber amplifier (EDFA) (Amonics, Model AEDFA-PA-35-B-FA) was used to boost the carrier power up to ~10 dBm. This optical carrier signal was launched into a dual polarization (DP) *I/Q* optical modulator

Optics EXPRESS

(SHF Communication Technologies AG, Model SHF 46215B DP-QAM) for data modulation. A modulated 28-GBd 16QAM optical signal was created using an arbitrary waveform generator (AWG) (Keysight Technologies, Model M8195A). The signal was amplified using another EDFA (Amonics, Model AEDFA-BO-23-B-FA) and transmitted for both B2B configuration and over 100-km of SSMF. Finally, after optimizing the power levels using an EDFA and a variable optical attenuator (VOA) (Agilent, Model 8156A), the received signal was processed by an integrated optical modulation analyzer (OMA) (Keysight Technologies, Model N4392A).

3. Results and discussion

3.1. InAs/InP QDot laser performance

Figure 2(a) shows the optical lasing spectra for devices with cavity lengths of 1000 μm, 1500 μm and 2000 μm, which exhibit corresponding center wavelengths of 1540 nm, 1550 nm and 1560 nm, respectively. Since the modal mirror loss for shorter cavity lengths is larger than that in longer devices they require larger gain to reach threshold. This higher gain is obtained at higher current densities and shorter wavelengths, resulting in the shorter devices lasing at shorter wavelength. The QDot laser at the cavity length of 1500 μm has a 10-dB comb bandwidth of 12.6 nm, providing 56 channels with an optical signal-to-noise ratio of more than 35 dB at 0.03 nm resolution bandwidth. Figure 2(b) shows the optical output spectrum as a function of injection current. Higher injection current results in higher Joule heating in the active region of the device, which causes the shift to longer wavelength. RF mode beating spectra for cavity lengths of 1000 μm, 1500 μm, and 2000 μm are presented in Fig. 2(c), showing sharp fundamental RF beating frequencies at 42.51 GHz, 28.45 GHz, and 21.37 GHz, respectively. All of them show a signal to noise floor ratio larger than 40 dB. The 3-dB mode beating RF linewidth for all lines simultaneously is 1.3 kHz at 28.45 GHz, and such an extremely narrow linewidth leads to excellent pulse-to-pulse timing jitter value (3.0 fs) [32].

To maximize spectral efficiency at a symbol rate of 28-GBd the QDot laser with a cavity length of 1500 μm, corresponding to a RF beating frequency of 28.45 GHz, was chosen for the detailed system performance study. Figure 3(a) shows the RIN spectra in the frequency range from 10 MHz to 20 GHz for both the whole lasing spectrum and three filtered channels. We obtain an integrated average RIN value of −167.988 dB/Hz for the whole laser, with the upper bound set by the instrument limited RIN measurement floor. When selecting only a single lasing line using a narrow optical bandpass filter, the integrated average RIN value increases due to the effect of mode partition noise, which is the result of competition for the common injected carrier population between the different longitudinal lasing modes. For example, the filtered channel at 1553.064 nm has a RIN value of −133.304 dB/Hz. The QDot-MLL exhibits a flat RIN in the 4–20 GHz range because the relaxation oscillations are strongly damped due to higher nonlinear gain introduced by intraband phenomena (spectral hole burning or carrier heating) or carrier transport in QDot structures [49]. Figure 3(b) shows the measured integrated average RIN for individually filtered comb lines. The average of integrated RIN values for the 56 filtered individual channels in the frequency range from 10 MHz to 20 GHz is −130.064 dB/Hz, ranging from −125.015 dB/Hz to −133.304 dB/Hz. In comparison we observe average RIN values of −126 dB/Hz for QDash lasers grown and processed at the same time. Figure 3(c) shows a comparison of the frequency noise spectra from three filtered channels at 1548.298 nm, 1550.128 nm and 1553.064 nm. A strongly suppressed phase noise is observed over the entire frequency range of the carrier offset. The performance is believed to be due to the low amplified spontaneous emission (ASE) noise and low confinement factor properties of the QDot-MLL material. Figure 3(d) shows the optical linewidth of each of the filtered individual channels from 1544.01 nm to 1556.561 nm at 400 mA and 17°C. The average optical linewidth of all modes is 4.394 MHz, measured using the OEWaves system. The significant scatter on the data is likely a consequence of environmental noise in the system, accentuated by the fact that the laser was not

Optics EXPRESS

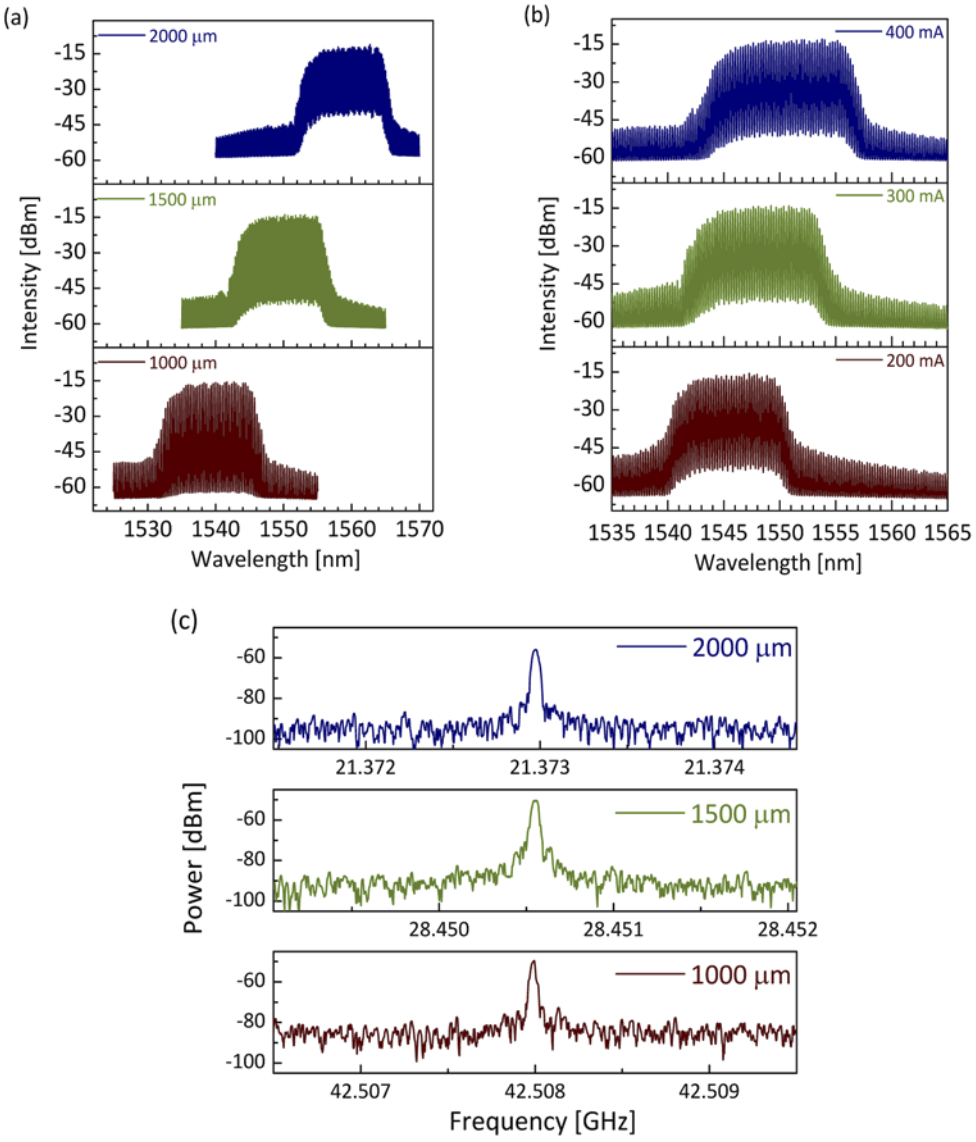

Fig. 2. (a) Optical output spectra of the QDot-MLL with cavity lengths of 1000 µm, 1500 µm, and 2000µm, measured at 400 mA and 17°C (resolution bandwidth (RBW): 0.03 nm); (b) Optical output spectra as a function of injection current for a cavity length of 1500 µm, measured at 200 mA, 300 mA, and 400 mA. (RBW: 0.03 nm); and (c) RF mode beating frequency for cavity lengths of 1000 µm, 1500 µm, and 2000µm (Span: 3 MHz, RBW: 47 kHz, VBW: 10 kHz).

directly bonded onto a carrier. A parabolic dependence related to the residual timing fluctuations that depend on timing jitter can be clearly observed.

3.2. Data transmission performance

Figure 4(a) shows the experimental setup for the 16QAM data transmission. At the dual polarization (DP) *I/Q* optical modulator side (T_X), a 28-GBd 16QAM base-band signal is created by using an arbitrary waveform generator (AWG, 65 GSa/s, 25 GHz bandwidth) generating a

Optics EXPRESS

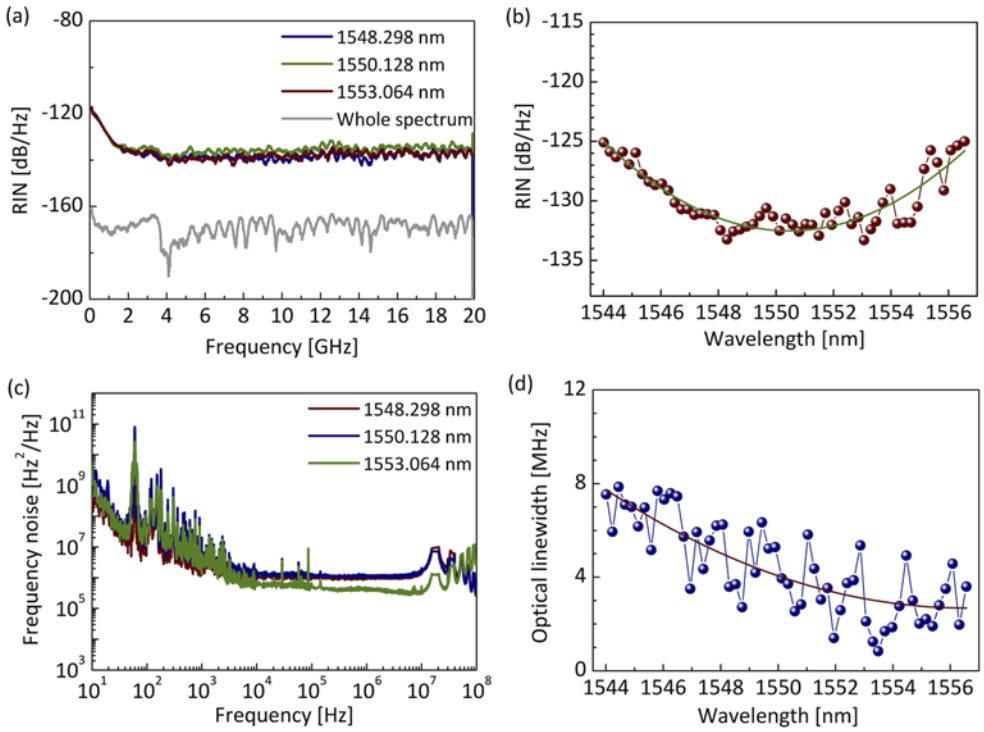

Fig. 3. (a) Measured RIN for the whole laser and three filtered channels in the frequency range from 10 MHz to 20 GHz; (b) Measured integrated average RIN of the QDot-MLL for individually filtered comb lines in the frequency range from 10 MHz to 20 GHz. The solid line is a parabolic fit; (c) A comparison of the frequency noise spectra from three filtered wavelength channels of 1548.298 nm, 1550.128 nm and 1553.064 nm; and (d) Optical linewidth of the filtered individual channels from 1544.01 nm to 1556.561 nm at 400 mA and 17°C. The solid line is a parabolic fit.

pseudo-random bit sequence (PRBS) with a pattern length of $2^{15}-1$ bits at a symbol rate of 28 Gbit/s non-return to zero (NRZ) on two uncorrelated channels (*IY/IX*). A root-raised-cosine (RRC) filter is applied with the roll-factor of 0.35 for Nyquist pulse filtering. Thermally stable nested lithium niobate ($LiNbO_3$) Mach-Zehnder modulators (23 GHz bandwidth) that constitute the *I/Q* optical modulator are driven by the AWG for data modulation. The encoded optical signal is transmitted for both B2B configuration and over 100-km SSMF, respectively. At the receiver side (R_X), the encoded signal is amplified by $EDFA_3$ and $OBPF_2$ is used to filter out the ASE from the EDFA. A variable optical attenuator (VOA) can be added before the optical modulation analyzer to control the received optical power. The Keysight optical modulation analyzer (OMA, 63 GSa/s, 23 GHz bandwidth) coherently receives the signals using a free-running local oscillator (LO). The intrinsic linewidth of the LO is approximately 10 kHz. Combined with the vector signal analyzer software package offered by the OMA [34], the sampled waveforms are processed with front-end correction and de-skewing, then compensated for chromatic dispersion and frequency offset. Afterwards, the signals are match-filtered and synchronized for time-domain equalization. A 51-tap adaptive blind equalizer based on the Kalman filtering for phase tracking [50,51] is employed to compensate for the phase noise simultaneously [2]. Finally, the output 16QAM signal is decoded for error-vector-magnitude (EVM) measurement and BER evaluation. The BER performance is evaluated based on the EVM measurement [52,53].

Optics EXPRESS

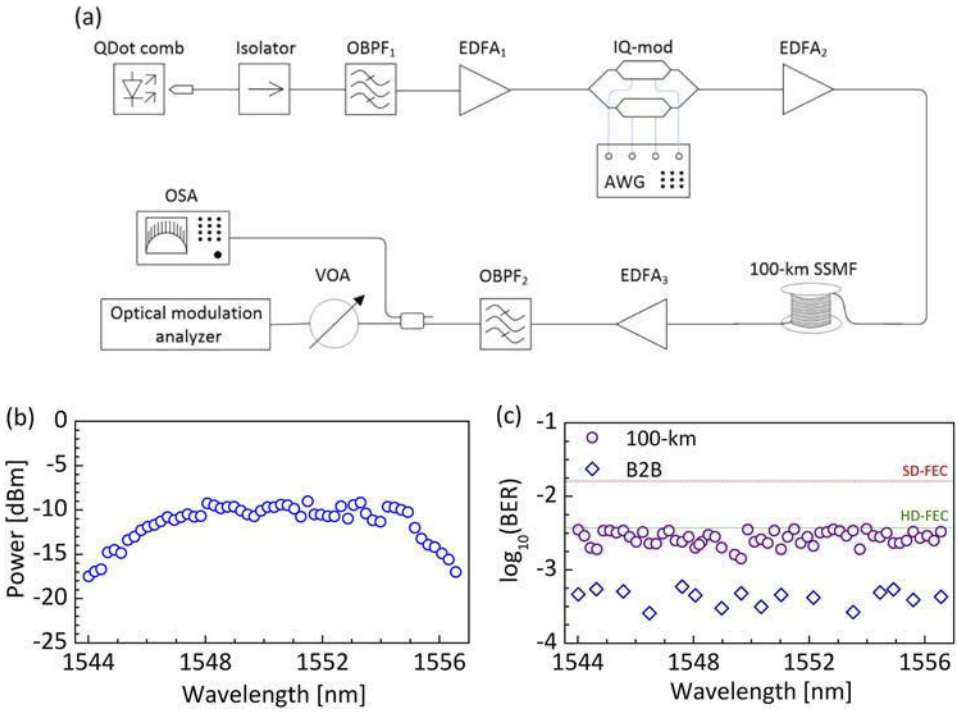

Fig. 4. (a) 16QAM data transmission setup with the DP *I/Q* optical modulator (T_X) and the receiver (R_X). $EDFA_3$ is only used for 100-km SSMF transmission; (b) Power level for each filtered comb line after $OBPF_1$; and (c) BER evaluation for B2B and after 100-km of SSMF transmission. All the selected channels are below the SD-FEC limit (BER = 2.0×10^{-2}) and HD-FEC limit (BER = 3.8×10^{-3}).

The performance of coherent communications highly depends on the properties of optical source, such as the number of comb lines, the power per line, the optical signal-to-noise ratio, the optical linewidth, and the RIN [5]. Figure 4(b) shows the power level for each filtered comb line with all the comb lines above −18 dBm. To avoid nonlinearities, the total power entering the SSMF is limited to 10 dBm [3,34]. The $EDFA_3$ is operated in constant-output-power mode thus the power levels at the input of the OMA do not vary significantly from channel to channel. Figure 4(c) shows the BER performance of each channel at the same received optical power of −10 dBm for all individual channels after 100-km SSMF, along with the back-to-back BER for 16 randomly selected channels. All selected channels exhibit BERs below the hard-decision FEC (HD-FEC) limit (7% overhead, BER = 3.8×10^{-3}) [54] after B2B and 100-km SSMF transmission (chromatic dispersion of 17 ps/nm/km). Figure 5(a) shows the dependence of BER evaluation on received optical power for the carriers at 1549.668 nm and 1552.180 nm for B2B and after 100-km of SSMF transmission. A VOA before the optical modulation analyzer was used to control the received optical power. The BER floors can be observed around −15 dBm. Figure 5(b) shows constellation diagrams for the channel at 1552.180 nm after B2B and 100-km SSMF transmission. In the B2B configuration, we attain a signal quality ($Q^2[\text{dB}] \approx 20log_{10}\left(\frac{1}{EVM}\right)$) [52,53] approaching 20.91 dB, dropping to near 18.77 dB when transmitting the modulated comb line through 100-km SSMF. A very small phase noise for B2B transmission in Fig. 5(b) is attributed to residual phase noise that is still left after phase tracking [55]. The aggregate line-rate data transmission capacity of the system is 12.544 Tbit/s (16QAM 56 × 28-GBd PDM).

Optics EXPRESS

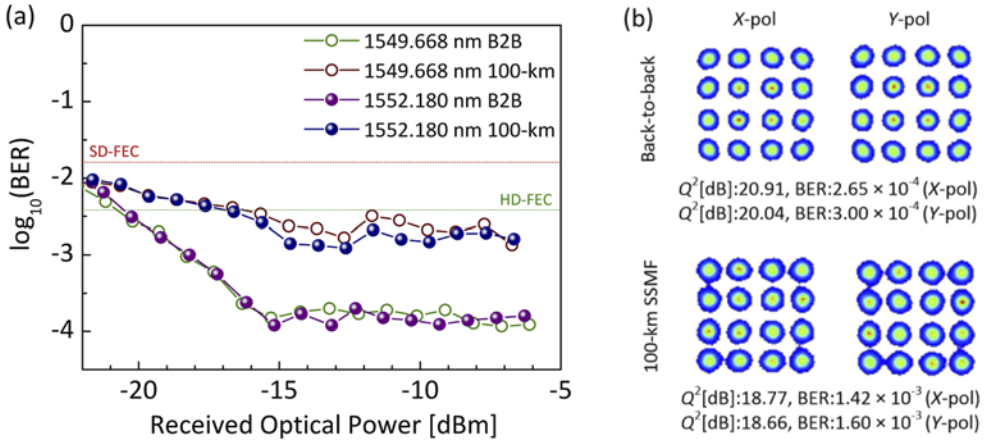

Fig. 5. (a) BER evaluation versus received optical power for B2B and after 100-km of SSMF transmission using the comb lines located at 1549.668 nm and 1552.180 nm; and (b) Constellation diagram obtained for selected channel at 1552.180 nm for both *X*- and *Y*-polarization after B2B and 100-km of SSMF transmission. The color indicates the relative density of symbols detected in the complex plane, with red indicating a higher density and blue a lower density.

4. Conclusion

We have measured in detail the performance of an InAs/InP QDot-MLL with 56 individual channels at a mode spacing of 28.45 GHz. The average of integrated RIN values for the 56 filtered individual channels is −130.064 dB/Hz and the average optical linewidth is 4.394 MHz. By employing 56 wavelength channels as optical carriers, 12.544 Tbit/s 16QAM aggregate line-rate data transmission capacity is demonstrated with the base modulation rate of 28-GBd over 100-km standard single-mode fiber. This performance is achieved without any form of feedback to control the laser linewidth. This represents the highest line-rate achieved through a chip-scale comb generator using a single-section semiconductor MLL and 16QAM modulation format without any external feedback schemes. These achievements may be a significant step towards low-cost, high wavelength channel count light sources for large-scale optical networking systems.

Acknowledgments. The authors would like to acknowledge the support of National Research Council Canada's high throughput and secure networks (HTSN) research program.

Disclosures. The authors declare no conflicts of interest.

Data availability. Data underlying the results presented in this paper are not publicly available at this time but may be obtained from the authors upon reasonable request.

References

1. B. Corcoran, M. Tan, X. Xu, A. Boes, J. Wu, T. G. Nguyen, S. T. Chu, B. E. Little, R. Morandotti, A. Mitchell, and D. J. Moss, "Ultra-dense optical data transmission over standard fibre with a single chip source," Nat. Commun. **11**(1), 2568 (2020).
2. L. Lundberg, M. Mazur, A. Mirani, B. Foo, J. Schröder, V. Torres-Company, M. Karlsson, and P. A. Andrekson, "Phase-coherent lightwave communications with frequency combs," Nat. Commun. **11**(1), 201 (2020).
3. P. Marin-Palomo, J. N. Kemal, T. J. Kippenberg, W. Freude, S. Randel, and C. Koos, "Performance of chip-scale optical frequency comb generators in coherent WDM communications," Opt. Express **28**(9), 12897–12910 (2020).
4. Y. Zhang, R. Zhang, Q. Zhu, Y. Yuan, and Y. Su, "Architecture and devices for silicon photonic switching in wavelength, polarization and mode," J. Lightwave Technol. **38**(2), 215–225 (2020).
5. J. Pfeifle, V. Vujicic, R. T. Watts, P. C. Schindler, C. Weimann, R. Zhou, W. Freude, L. P. Barry, and C. Koos, "Flexible terabit/s Nyquist-WDM super-channels using a gain-switched comb source," Opt. Express **23**(2), 724–738 (2015).

Optics EXPRESS

6. Ó. B. Helgason, A. Fülöp, J. Schröder, P. A. Andrekson, and A. M. Weiner, "Superchannel engineering of microcombs for optical communications," J. Opt. Soc. Am. B **36**(8), 2013–2022 (2019).
7. P. Marin-Palomo, J. N. Kemal, M. Karpov, A. Kordts, J. Pfeifle, M. H. Pfeiffer, P. Trocha, S. Wolf, V. Brasch, and M. H. Anderson, "Microresonator-based solitons for massively parallel coherent optical communications," Nature **546**(7657), 274–279 (2017).
8. A. Fülöp, M. Mazur, A. Lorences-Riesgo, Ó. B. Helgason, P.-H. Wang, Y. Xuan, D. E. Leaird, M. Qi, P. A. Andrekson, and A. M. Weiner, "High-order coherent communications using mode-locked dark-pulse Kerr combs from microresonators," Nat. Commun. **9**(1), 1598 (2018).
9. B. Shen, L. Chang, J. Liu, H. Wang, Q.-F. Yang, C. Xiang, R. N. Wang, J. He, T. Liu, and W. Xie, "Integrated turnkey soliton microcombs," Nature **582**(7812), 365–369 (2020).
10. B. Stern, X. Ji, Y. Okawachi, A. L. Gaeta, and M. Lipson, "Battery-operated integrated frequency comb generator," Nature **562**(7727), 401–405 (2018).
11. A. S. Raja, J. Liu, N. Volet, R. N. Wang, J. He, E. Lucas, R. Bouchandand, P. Morton, J. Bowers, and T. J. Kippenberg, "Chip-based soliton microcomb module using a hybrid semiconductor laser," Opt. Express **28**(3), 2714–2721 (2020).
12. S. J. Herr, V. Brasch, J. Szabados, E. Obrzud, Y. Jia, S. Lecomte, K. Buse, I. Breunig, and T. Herr, "Frequency comb up-and down-conversion in synchronously driven $\chi^{(2)}$ optical microresonators," Opt. Lett. **43**(23), 5745–5748 (2018).
13. M. Zhang, B. Buscaino, C. Wang, A. Shams-Ansari, C. Reimer, R. Zhu, J. M. Kahn, and M. Lončar, "Broadband electro-optic frequency comb generation in a lithium niobate microring resonator," Nature **568**(7752), 373–377 (2019).
14. J. Lin, H. Sepehrian, Y. Xu, L. A. Rusch, and W. Shi, "Frequency comb generation using a CMOS compatible SiP DD-MZM for flexible networks," IEEE Photonics Technol. Lett. **30**(17), 1495–1498 (2018).
15. J. Alexander, P. Morrissey, H. Yang, M. Yang, P. Marraccini, B. Corbett, and F. Peters, "Monolithically integrated low linewidth comb source using gain switched slotted Fabry-Perot lasers," Opt. Express **24**(8), 7960–7965 (2016).
16. E. U. Rafailov, M. A. Cataluna, and W. Sibbett, "Mode-locked quantum-dot lasers," Nat. Photonics **1**(7), 395–401 (2007).
17. Z. G. Lu, J. R. Liu, S. Raymond, P. J. Poole, P. J. Barrios, and D. Poitras, "312-fs pulse generation from a passive C-band InAs/InP quantum dot mode-locked laser," Opt. Express **16**(14), 10835–10840 (2008).
18. Z. G. Lu, J. R. Liu, P. J. Poole, S. Raymond, P. J. Barrios, D. Poitras, G. Pakulski, P. Grant, and D. Roy-Guay, "An L-band monolithic InAs/InP quantum dot mode-locked laser with femtosecond pulses," Opt. Express **17**(16), 13609–13614 (2009).
19. S. Chen, W. Li, J. Wu, Q. Jiang, M. Tang, S. Shutts, S. N. Elliott, A. Sobiesierski, A. J. Seeds, and I. Ross, "Electrically pumped continuous-wave III–V quantum dot lasers on silicon," Nat. Photonics **10**(5), 307–311 (2016).
20. M. Tang, J.-S. Park, Z. Wang, S. Chen, P. Jurczak, A. Seeds, and H. Liu, "Integration of III-V lasers on Si for Si photonics," Prog. Quantum. Electron. **66**, 1–18 (2019).
21. R. Helkey, A. A. Saleh, J. Buckwalter, and J. E. Bowers, "High-performance photonic integrated circuits on silicon," IEEE J. Sel. Top. Quantum Electron. **25**(5), 1–15 (2019).
22. S. Liu, X. Wu, D. Jung, J. C. Norman, M. Kennedy, H. K. Tsang, A. C. Gossard, and J. E. Bowers, "High-channel-count 20 GHz passively mode-locked quantum dot laser directly grown on Si with 4.1 Tbit/s transmission capacity," Optica **6**(2), 128–134 (2019).
23. S. P. Duill, S. G. Murdoch, R. T. Watts, R. Rosales, A. Ramdane, P. Landais, and L. P. Barry, "Simple dispersion estimate for single-section quantum-dash and quantum-dot mode-locked laser diodes," Opt. Lett. **41**(24), 5676–5679 (2016).
24. K. Merghem, A. Akrout, A. Martinez, G. Aubin, A. Ramdane, F. Lelarge, and G.-H. Duan, "Pulse generation at 346 GHz using a passively mode locked quantum-dash-based laser at 1.55 μm," Appl. Phys. Lett. **94**(2), 021107 (2009).
25. R. Rosales, K. Merghem, A. Martinez, A. Akrout, J.-P. Tourrenc, A. Accard, F. Lelarge, and A. Ramdane, "InAs/InP quantum-dot passively mode-locked lasers for 1.55-μm applications," IEEE J. Sel. Top. Quantum Electron. **17**(5), 1292–1301 (2011).
26. P. Marin-Palomo, J. N. Kemal, P. Trocha, S. Wolf, K. Merghem, F. Lelarge, A. Ramdane, W. Freude, S. Randel, and C. Koos, "Comb-based WDM transmission at 10 Tbit/s using a DC-driven quantum-dash mode-locked laser diode," Opt. Express **27**(22), 31110–31129 (2019).
27. Y. X. Mao, Z. G. Lu, J. R. Liu, P. J. Poole, and G. C. Liu, "Pulse timing jitter estimated from optical phase noise in mode-locked semiconductor quantum dash lasers," J. Lightwave Technol. **38**(17), 4787–4793 (2020).
28. G. Vedala, M. Al-Qadi, M. O'Sullivan, J. Cartledge, and R. Hui, "Phase noise characterization of a QD-based diode laser frequency comb," Opt. Express **25**(14), 15890–15904 (2017).
29. A.-Q. Mustafa, C. Laperle, D. Charlton, M. O'Sullivan, C. Xie, and R. Hui, "Multichannel 16-QAM single-sideband transmission and Kramers–Kronig detection using a single QD-MLL as the light source," J. Lightwave Technol. **38**(22), 6163–6169 (2020).
30. V. Vujicic, A. P. Anthur, A. Saljoghei, V. Panapakkam, R. Zhou, Q. Gaimard, K. Merghem, F. Lelarge, A. Ramdane, and L. P. Barry, "Mitigation of relative intensity noise of quantum dash mode-locked lasers for PAM4 based optical interconnects using encoding techniques," Opt. Express **25**(1), 20–29 (2017).
31. V. Vujicic, C. Calo, R. Watts, F. Lelarge, C. Browning, K. Merghem, A. Martinez, A. Ramdane, and L. P. Barry, "Quantum dash mode-locked lasers for data centre applications," IEEE J. Sel. Top. Quantum Electron. **21**(6), 53–60 (2015).

Optics EXPRESS

32. Y. X. Mao, J. R. Liu, Z. G. Lu, C. Y. Song, and P. J. Poole, "Ultra-low timing jitter of quantum dash semiconductor comb lasers with self-injection feedback locking," IEEE J. Sel. Top. Quantum Electron. **25**(6), 1–7 (2019).
33. J. N. Kemal, P. Marin-Palomo, V. Panapakkam, P. Trocha, S. Wolf, K. Merghem, F. Lelarge, A. Ramdane, S. Randel, W. Freude, and C. Koos, "Coherent WDM transmission using quantum-dash mode-locked laser diodes as multi-wavelength source and local oscillator," Opt. Express **27**(22), 31164–31175 (2019).
34. J. N. Kemal, P. Marin-Palomo, K. Merghem, G. Aubin, F. Lelarge, A. Ramdane, S. Randel, W. Freude, and C. Koos, "32QAM WDM transmission at 12 Tbit/s using a quantum-dash mode-locked laser diode (QD-MLLD) with external-cavity feedback," Opt. Express **28**(16), 23594–23608 (2020).
35. T. Verolet, G. Aubin, Y. Lin, C. Browning, K. Merghem, F. Lelarge, C. Calo, A. Delmade, K. Mekhazni, and E. Giacoumidis, "Mode locked laser phase noise reduction under optical feedback for coherent DWDM communication," J. Lightwave Technol. **38**(20), 5708–5715 (2020).
36. C. Browning, T. Verolet, Y. Lin, G. Aubin, F. Lelarge, A. Ramdane, and L. P. Barry, "56 Gb/s/λ over 1.3 THz frequency range and 400G DWDM PAM-4 transmission with a single quantum dash mode-locked laser source," Opt. Express **28**(15), 22443–22449 (2020).
37. G. C. Liu, Z. G. Lu, J. R. Liu, Y. X. Mao, M. Vachon, C. Y. Song, P. J. Barrios, and P. J. Poole, "Passively mode-locked quantum dash laser with an aggregate 5.376 Tbit/s PAM-4 transmission capacity," Opt. Express **28**(4), 4587–4593 (2020).
38. Z. G. Lu, J. R. Liu, P. J. Poole, Y. X. Mao, J. Weber, G. C. Liu, and P. J. Barrios, "InAs/InP quantum dash semiconductor coherent comb lasers and their applications in optical networks," J. Lightwave Technol. **39**(12), 3751–3760 (2021).
39. Z. G. Lu, J. R. Liu, Y. X. Mao, C. Y. Song, J. Weber, and P. J. Poole, "12.032 Tbit/s coherent transmission using an ultra-narrow linewidth qantum dot 34.46-GHz C-Band coherent comb laser," in *Next-Generation Optical Communication: Components, Sub-Systems, and Systems VIII*, G. Li and X. Zhou, eds. (SPIE, 2019), p. 23.
40. Q. Zou, K. Merghem, S. Azouigui, A. Martinez, A. Accard, N. Chimot, F. Lelarge, and A. Ramdane, "Feedback-resistant p-type doped InAs/InP quantum-dash distributed feedback lasers for isolator-free 10 Gb/s transmission at 1.55 μm," Appl. Phys. Lett. **97**(23), 231115 (2010).
41. P. J. Poole, K. Kaminska, P. J. Barrios, Z. G. Lu, and J. R. Liu, "Growth of InAs/InP-based quantum dots for 1.55 μm laser applications," J. Cryst. Growth **311**(6), 1482–1486 (2009).
42. Z. G. Lu, J. R. Liu, P. J. Poole, C. Y. Song, and S. D. Chang, "Ultra-narrow linewidth quantum dot coherent comb lasers with self-injection feedback locking," Opt. Express **26**(9), 11909–11914 (2018).
43. Z. G. Lu, J. R. Liu, C. Y. Song, J. Weber, Y. X. Mao, S. D. Chang, H. P. Ding, P. J. Poole, P. J. Barrios, and D. Poitras, "High performance InAs/InP quantum dot 34.462-GHz C-band coherent comb laser module," Opt. Express **26**(2), 2160–2167 (2018).
44. C. Gilfert, V. Ivanov, N. Oehl, M. Yacob, and J. Reithmaier, "High gain 1.55 μm diode lasers based on InAs quantum dot like active regions," Appl. Phys. Lett. **98**(20), 201102 (2011).
45. T. Sadeev, D. Arsenijević, and D. Bimberg, "Comparison of dynamic properties of InP/InAs quantum-dot and quantum-dash lasers," Appl. Phys. Lett. **109**(16), 161104 (2016).
46. N. A. Jahan, C. Hermannstädter, J.-H. Huh, H. Sasakura, T. J. Rotter, P. Ahirwar, G. Balakrishnan, K. Akahane, M. Sasaki, and H. Kumano, "Temperature dependent carrier dynamics in telecommunication band InAs quantum dots and dashes grown on InP substrates," J. Appl. Phys. **113**(3), 033506 (2013).
47. A. J. Zilkie, J. Meier, M. Mojahedi, P. J. Poole, P. Barrios, D. Poitras, T. J. Rotter, C. Yang, A. Stintz, and K. J. Malloy, "Carrier dynamics of quantum-dot, quantum-dash, and quantum-well semiconductor optical amplifiers operating at 1.55 μm," IEEE J. Quantum Electron. **43**(11), 982–991 (2007).
48. P. J. Poole, "InP-based quantum dot lasers, " in *Advances in Semiconductor Lasers*, J. J. Coleman, A.C. Bryce, and C. Jagadish, Editors. 2012, Academic Press. pp. 419–453.
49. F. Lelarge, B. Dagens, J. Renaudier, R. Brenot, A. Accard, F. van Dijk, D. Make, O. Le Gouezigou, J.-G. Provost, and F. Poingt, "Recent advances on InAs/InP quantum dash based semiconductor lasers and optical amplifiers operating at 1.55 μm," IEEE J. Sel. Top. Quantum Electron. **13**(1), 111–124 (2007).
50. T. Marshall, B. Szafraniec, and B. Nebendahl, "Kalman filter carrier and polarization-state tracking," Opt. Lett. **35**(13), 2203–2205 (2010).
51. B. Szafraniec, T. S. Marshall, and B. Nebendahl, "Performance monitoring and measurement techniques for coherent optical systems," J. Lightwave Technol. **31**(4), 648–663 (2013).
52. R. A. Shafik, M. S. Rahman, and A. R. Islam, "On the extended relationships among EVM, BER and SNR as performance metrics," in *Proceedings of International Conference on Electrical and Computer Engineering* (2006), pp. 408–411.
53. R. Schmogrow, B. Nebendahl, M. Winter, A. Josten, D. Hillerkuss, S. Koenig, J. Meyer, M. Dreschmann, M. Huebner, and C. Koos, "Error vector magnitude as a performance measure for advanced modulation formats," IEEE Photonics Technol. Lett. **24**(1), 61–63 (2012).
54. H. Hu, F. Da Ros, M. Pu, F. Ye, K. Ingerslev, E. P. da Silva, M. Nooruzzaman, Y. Amma, Y. Sasaki, and T. Mizuno, "Single-source chip-based frequency comb enabling extreme parallel data transmission," Nat. Photonics **12**(8), 469–473 (2018).
55. T. Pfau, S. Hoffmann, and R. Noé, "Hardware-efficient coherent digital receiver concept with feedforward carrier recovery for *M*-QAM constellations," J. Lightwave Technol. **27**(8), 989–999 (2009).